OCAM2S: an integral shutter ultrafast and low noise wavefront sensor camera for laser guide stars adaptive optics systems

Gach[1,a,b], Jean-Luc ; Feautrier[a,c] , Philippe ; Buey[d], Tristan; Rousset[d], Gérard ;Gendron[d], Eric; Morris[e], Tim; Basden[e], Alastair; Stadler[a,c], Eric ; Myers[e], Richard; Vidal[d], Fabrice; Chemla[f], Fanny.

[a]First Light Imaging S.A.S. 100, Route des houillères, 13590 Meyreuil, France;
[b]Aix Marseille Université, CNRS, LAM (Laboratoire d'Astrophysique de Marseille) UMR 7326, 13388 Marseille, France ;
[c]IPAG, Domaine Universitaire, 414 rue de la Piscine, BP 53 38041 Grenoble Cedex 9, France;
[d]LESIA, Observatoire de Paris, 5 place Jules Janssen, 92195 MEUDON Cedex, France;
[e]CfAI Department of Physics, Durham University, South Road, Durham DH1 3LE United Kingdom;
[f]GEPI, Observatoire de Paris, 5 place Jules Janssen, 92195 Meudon Cedex, France;

ABSTRACT

To date, the OCAM2 system has demonstrated to be the fastest and lowest noise production ready wavefront sensor, achieving 2067 full frames per second with subelectron readout noise. This makes OCAM2 the ideal system for natural as well as continuous wave laser guide star wavefront sensing. In this paper we present the new gated version of OCAM2 named OCAM2-S, using E2V's CCD219 sensor with integral shutter. This new camera offers the same superb characteristics than OCAM2 both in terms of speed and readout noise but also offers a shutter function that makes the sensor only sensitive to light for very short periods, at will. We will report on gating time and extinction ratio performances of this new camera. This device opens new possibilities for Rayleigh pulsed lasers adaptive optics systems. With a shutter time constant well below 1 microsecond, this camera opens new solutions for pulsed sodium lasers with backscatter suppression or even spot elongation minimization for ELT LGS. This camera has been successfully used for the first time on the CANARY instrument on the William Herschel Telescope. The final phase of CANARY is a demonstrator of a single MOAO channel for the proposed EAGLE instrument on the future European ELT. We will report on-sky performance with this instrument.

Keywords: adaptive optics, EMCCD, Electron Multiplying CCD, L3Vision CCD, L3CCD, photon counting, low readout noise, laser guide star, wavefront sensor, LGS, WFS, MOAO.

1. INTRODUCTION

The success of the next generation of ESO (European Southern Observatory) instruments (e.g. VLT SPHERE, MUSE, HAWK-I) for 8 to 10-m class telescopes will depend on the ability of Adaptive Optics (AO) systems to provide excellent image quality and stability. This will be achieved by increasing the sampling and correction of the wave front error in both spatial and time domains. For example, current Shack Hartmann systems require 40x40 sub-apertures at sampling rates above 1-1.5 kHz as opposed to 14x14 sub-apertures at 500 Hz for previous AO systems. Detectors of 240x240 pixels are required to provide spatial dynamics of 5-6 pixels per sub-aperture. Higher temporal-spatial sampling implies fewer photons per pixel therefore the need for much lower read noise (<<1e-) and negligible dark current (<< 1e-/pixel/frame) to detect and centroid on a small number of photons.

Numerous European astronomy institutions have teamed up in the OPTICON network [3], and obtained funds in the Joint Research Activity JRA2, "Fast Detectors for Adaptive Optics", from the European Commission to support the massive R&D effort to develop new detectors for adaptive optics applications. This development was jointly funded by ESO and OPTICON. After extensive market research culminating in a Call For Tender, *e2v technologies* was chosen to

[1] Jean-luc.gach@first-light.fr ; phone +33 (0)4 42612920 ;

develop a custom-designed detector based on an extension of their L3Vision [1] EMCCD technology. During this development, a speculative variant of the detector devoted to laser guide star wavefront sensing was developed and further tested with the help of the 7th European Union Framework Program (agreement N°226604).

2. THE CCD219 DESIGN

2.1. General structure

CCD219 was the name chosen by *e2v technologies* for this detector. The CCD219 is a derivative of the CCD220 [2], [3], [4] (schematic in Figure 1) which is a 24 µm square 240x240 pixels split frame transfer back illuminated L3Vision CCD. The image and store area (store is optically shielded) are built with 2-phase metal-buttressed parallel clock structures to enable fast line shifts in excess of 7 Mlines/s for total transfer time from image to store of 18 µs and low smearing of under 2% at 1,200 fps. Eight electron-multiplying L3Vision [1] registers operating at greater than 13 Mpixel/sec enable sub electron noise to be achieved at frame rates of 1,300 fps. Each pixel has an embedded shutter system consisting of an extra drain. To provide shutter routing, the two central lines of the device are inactive.

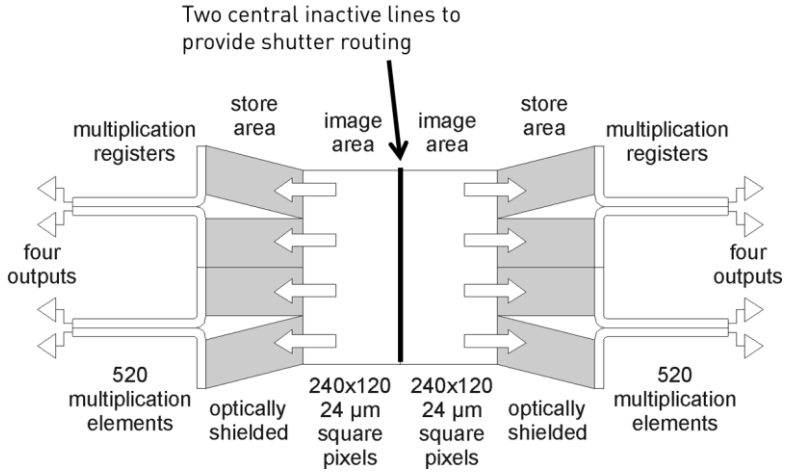

Figure 1: Schematic of e2v technologies 240x240 pixel L3Vision CCD219. Eight electron-multiplying (gain) registers are used to obtain sub electron noise at frame rates above 1300 fps. The two central lines are inactive to provide routing for the shutter system.

The store area is slanted out to make room for the standard serial registers (three phase clocking) to curve around (Figure 2) and provide space for the output circuitry. Each output has a 520 element 16 µm standard L3Vision gain register whose gain is controlled by the voltage of the multiplication phase. The output amplifier is a 2-stage source follower and of similar design to that employed on recent L3V CCDs (CCD97). The gain register is optimized for a gain of 500-600, a value typically expected for AO applications. With an expected output amplifier read out noise (RON) of 50e, this will provide an overall effective read noise of under 0.1 e- (50 e- RON/500 of gain register). The serial registers, gain registers, and output amplifiers are designed to operate up to 15 Mpixel/s to achieve a full goal frame rate of over 1,500 fps. Frame rates exceeding 2067 fps have been achieved so far with 18.6 Mpixel/s pixel rates [6].

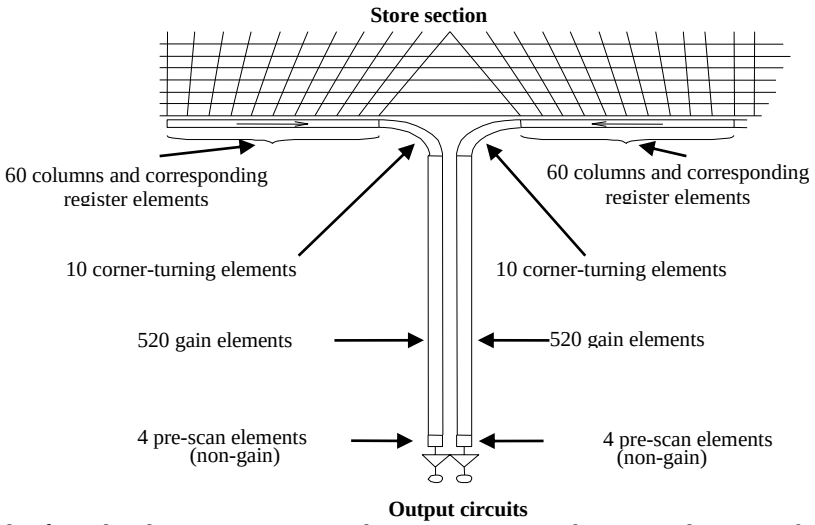

Figure 2. Details of serial and gain register. Two adjacent gain registers have a good gain matching since they are sharing the same silicon region

The device is made of high resistivity silicon (1500 Ω.cm), low resistivity types are not compatible with the shutter structure since the depleted regions and electric fields must extend far below the electrodes. The device is thinned to 40 µm and back-illuminated. This device will then exhibit a very good red response as seen in Figure 3.

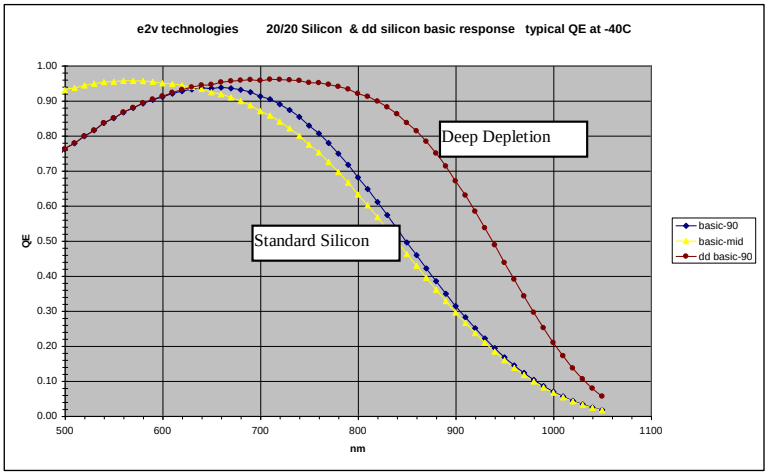

Figure 3 : Comparison of QE for a standard silicon device (basic-90/basic-mid) to that of a deep depletion device (dd basic-90). These curves are only typical and the curves of the final devices may differ.

2.2. Shutter design

The classical way to add shutter functionality to a CCD is to use interline transfer. But this method is not compatible with high quantum efficiency because half of the columns are metal masked. E2V has explored other ways to implement the shutter functionality, compatible with high QE devices. An extra drain has been added parallel to the device columns, and a buried p-layer in the high resistivity p-type silicon to make a charge confinement volume when the shutter is closed (see Figure 4)

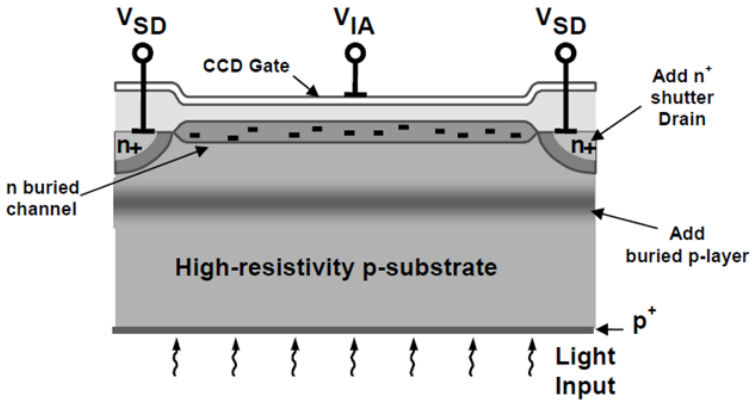

Figure 4 : The CCD219 pixel cross section. The n buried channel and the buried p layer will form a confinement volume for the charges when the shutter is open.

When the SD electrode is polarized to a low voltage, the CCD 219 works as a deep depleted CCD220: the charges generated in the bulk silicon are attracted by the electric field generated by the surrounding pixel electrode and moved to the interface of the p-silicon and the n-channel. In this phase the shutter is open. When the shutter drain voltage (V_{SD}) is raised to a sufficient level, the electric field generated by the SD drain will overcome the pixel field. The generated electrons will be attracted by the SD electrode and recombined, the charges are no more accumulated in the pixel well. The already accumulated charges will stay under the pixel electrode, the shutter is closed (see Figure 5)

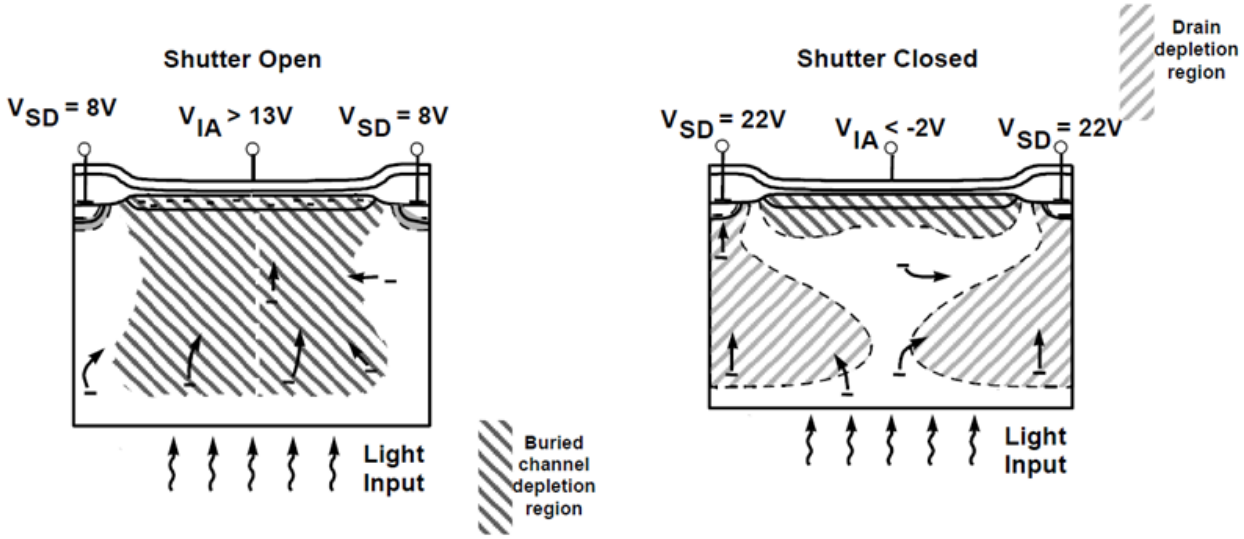

Figure 5 : The 219 underlying shutter mechanism, with depleted regions and charge collection mechanism, left shutter open and right shutter closed

This mechanism is wavelength dependent, since redder photons will penetrate deeper in the silicon, they will have more "chance" to reach the accumulation region than shorter wavelength photons. The extinction ratio (ratio of the charges accumulated when the shutter is open and the charges accumulated when the shutter is closed) also depends on the electrical field structure, and this is tuned by the buried P-layer doping level (see Figure 6)

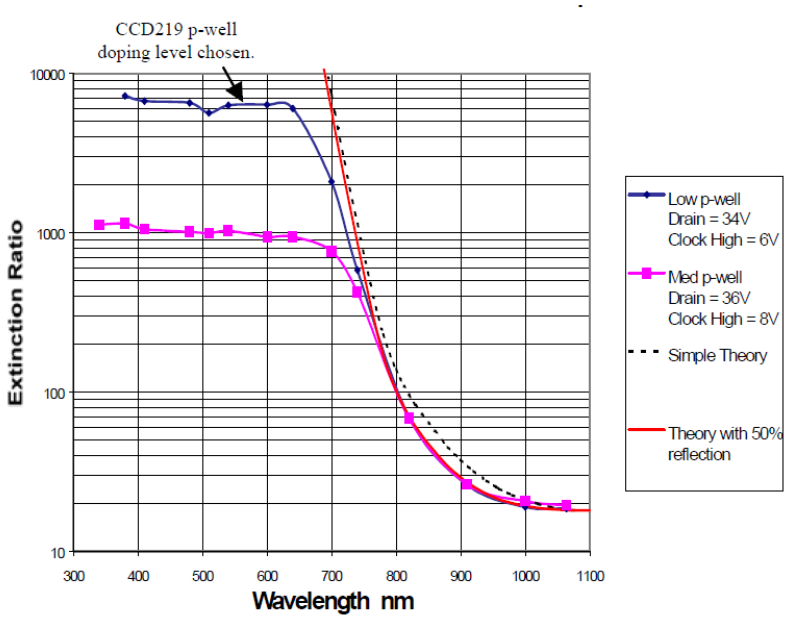

Figure 6 : Extinction ratio vs wavelength for various buried p-layer doping levels

The n-buried channel doping level must be adjusted accordingly and this results in a lower full well capacity of the pixels compared to a classical CCD device.

3. MEASURED SYSTEM PERFORMANCE

3.1. Full well capacity

To measure the full well capacity (FWC), we plot the photon transfer curve (PTC, see Figure 7). This gives access at the same time to the system gain, necessary to compute the FWC and the saturation level, where the PTC becomes nonlinear. The measurements demonstrate a mean system gain of 19.6 e^-/ADU and a mean saturation level at 4500 ADU, giving a FWC of 88 200 electrons. This is in accordance with the expected FWC, less than the CCD220 (270 000 e^- typical), due to the underlying shutter system.

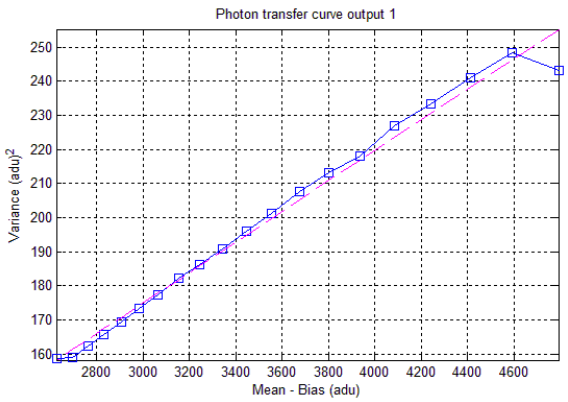

Figure 7 : OCAM2-S prototype amplifier 1 photon transfer curve showing the saturation level at 4600 ADU. The mean saturation on all the amplifiers is at 4500 ADU

3.2. System noise and dark

For this measurement, the system is placed in complete darkness and images are taken at various amplification gains. The final input referred noise is the standard image noise divided by the amplification gain. To convert this in electrons, we use the photon transfer curve to determine the system conversion ratio. The system exhibits a nice 0.11 electron noise at G=1000, and 0.24 electron at G=500 (see Figure 8 for the histograms)

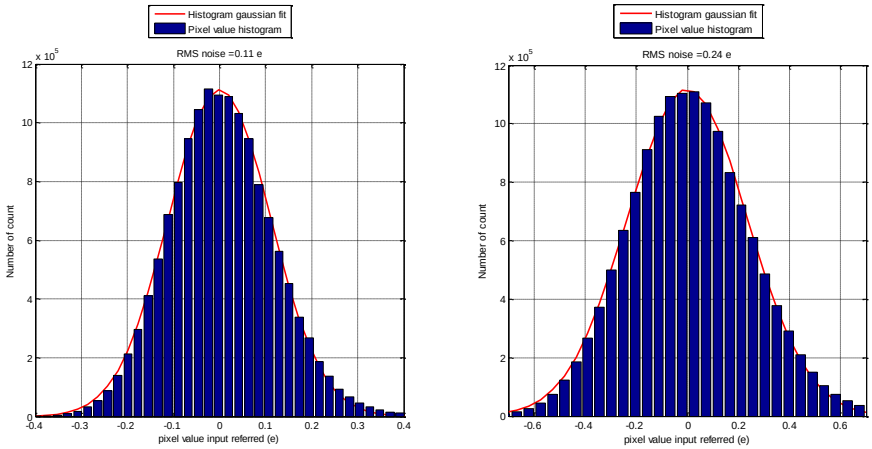

Figure 8 : OCAM2-S input referred noise histograms at various gains, left gain=1000, RMS noise = 0.11 electron, right gain=500, RMS noise = 0.24 electron

3.3. Shutter speed

To measure the shutter speed, the used method consists of generating a light pulse and sweeping the opening window of the shutter with respect to this pulse. For each sweep step, the image is recorded, this makes an image cube with intensity change profiles for each pixel. For each pixel we are the able to extract the intensity profile across the cube third dimension (see Figure 9). For each pixel, if the shutter opening and the light pulse are shorter than the frame exposure time, the intensity profile is then:

$$I(\tau) = \int_{Ft} P(t).S(\tau - t)dt \approx \int_{-\infty}^{+\infty} P(t).S(\tau - t)dt = [P * S](\tau)$$

Equation 1: the intensity profile function recorded vs the light pulse function and the shutter transmission function. I is the intensity, Ft is the frame time (CCD exposure time, 647 µs at 1503 FPS for OCAM2-S), t is time, τ is the time delay between the pulse and the shutter opening, P is the pulse intensity vs time function, S is the shutter transmission vs time function.

If the pulse function is short enough compared to the shutter opening function then *P(t)* can be considered as the Dirac delta function δ(t), and the Equation 1 can be reduced, giving directly access to the shutter transmission vs time function:

$$I(\tau) \approx [\delta * S](\tau) = S(\tau)$$

Equation 2 : If the pulse function is short enough, it can be considered as a Dirac delta function and gives directly access to the shutter transmission function *S(τ)*.

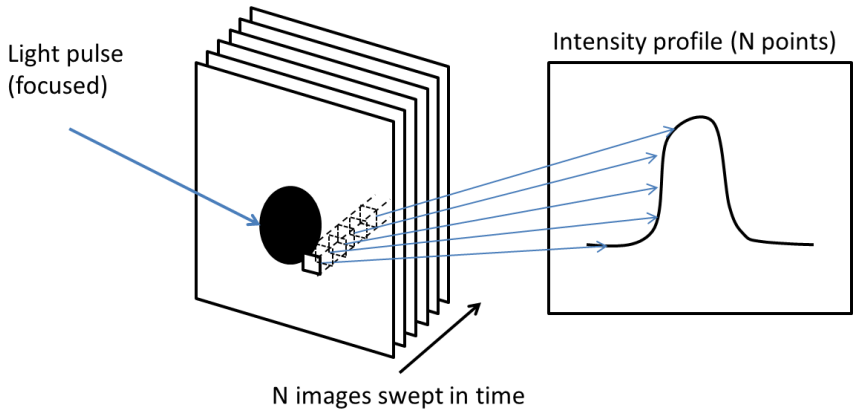

Figure 9 : The shutter speed measurement method. A light pulse is focused on the device. We take N images where the shutter opening is swept in time, each image gives a point in the intensity profile for a given area in the image.

In our case, we've used a laser diode pulse generator. The employed circuitry is inspired from [5], but instead of driving classical LEDs, we've used laser diodes that provide more light and will permit to focus larger spots on the detector. We've generated 20ns pulses, synchronous with the camera frame capture. For each step, the shutter opening time is swept by 9.21 ns which is the elementary tick of the shutter driver. Figure 10 shows the light pulse recorded by a fast Si amplified photodiode (Thorlabs PDA10A-EC – 150MHz bandwidth). The light pulse is square and has a width of 20ns which is more than 10 times shorter than the expected shutter speed. The global shutter response profile is obtained by averaging the pixel profiles across a square zone centered on the spot image. The spot image and intensity profile is shown in Figure 11.

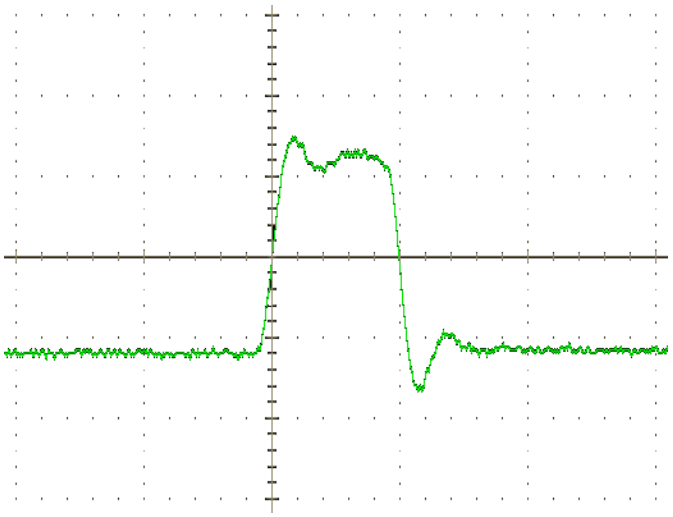

Figure 10: The recorded light pulse with a fast amplified photodiode (1V/div vertical scale, 20ns horizontal scale). The pulse width is 20 ns.

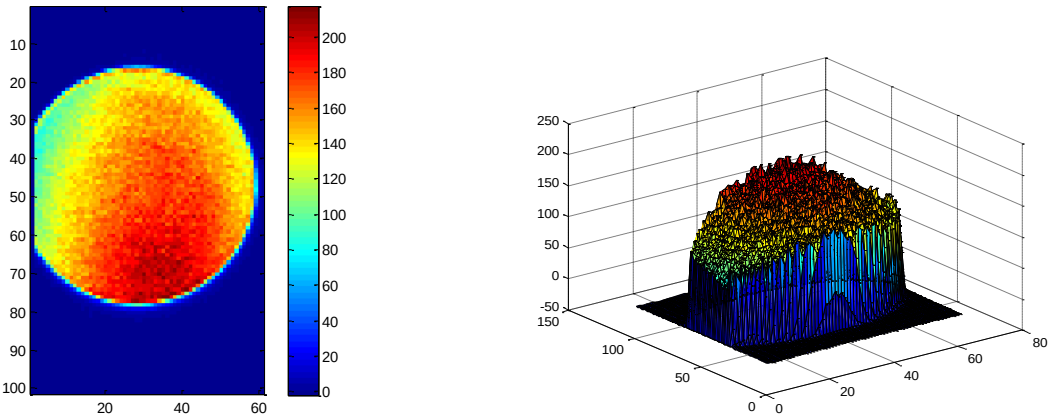

Figure 11 : The laser spot intensity profile (image of one amplifier of the CCD)

We've concentrated the measurements on the short pulses domain (<1µs) to determine the -3dB cutoff frequency of the shutter. Figure 12 left shows the shutter opening profile for various shutter opening times ranging from 100ns to 1µs. Plotting the peak transmission versus the shutter opening window width permits to determine precisely the -3dB cutoff frequency of the shutter system. It is in the range of 220 ns (see Figure 12 right) or 4.5 MHz. If we convert this in distance for laser ranging this gives a probing window depth of 33 m. This is faster than expected but the theory didn't take into account the metal buttressing of the parallel registers and the shutter response time is faster due to the low serial resistance of the parallel register.

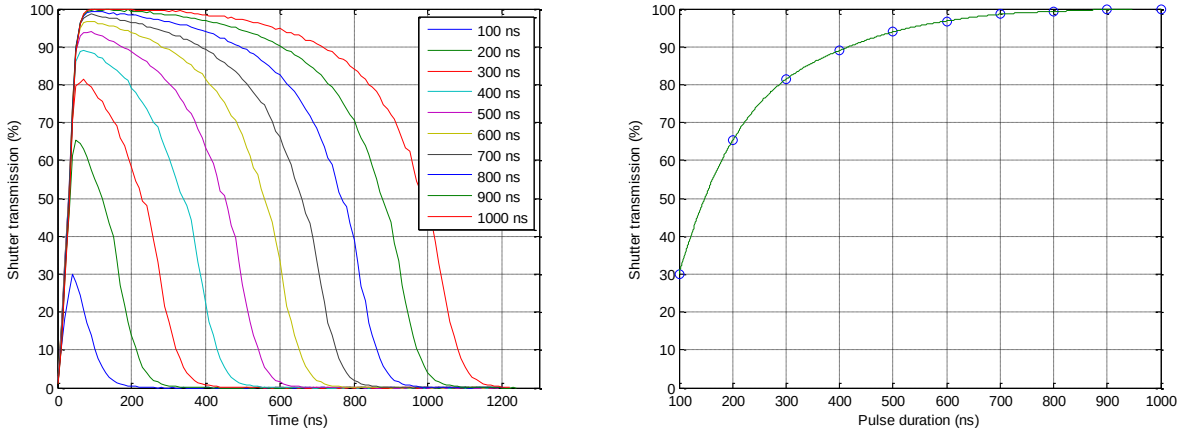

Figure 12 : The shutter opening profile at various speeds (left), and the peak opening vs shutter opening width (right)

3.4. Shutter extinction ratio

For this measurement, we've used the same pulse generator as exposed in 3.3, but with several laser sources pulsed at 40ns or 20ns for the highest power lasers. We pulse the shutter at 10000ns to obtain 100% throughput. We measure the signal level when the pulse is in the shutter window and when it is out of the shutter window. The ratio between the signal-in and signal-out gives the extinction ratio. For very faint signals when the pulse is out of the shutter window, we use the gain of the camera which has been carefully calibrated. Table 1 shows the wavelengths used, laser diodes and measured extinction ratio, Figure 13 shows the extinction curve vs wavelength.

Wavelength (nm)	manufacturer	MFG part number	Extinction
405	CNI	DL405-0.10	59880
450	OSRAM	PL450B	65840
520	OSRAM	PL520	57650
635	LASER COMPONENTS	ADL63054-TL	19325
660	OPNEXT	HL6544FM	4752
690	OPNEXT	HL6738MG	1642
785	THORLABS	QL7816S-B-L	87
850	THORLABS	L850P010	40
904	THORLABS	L904P010	27
980	THORLABS	L980P010	21

Table 1 : Wavelengths, laser diodes and measured extinction ratio of the OCAM2-S camera

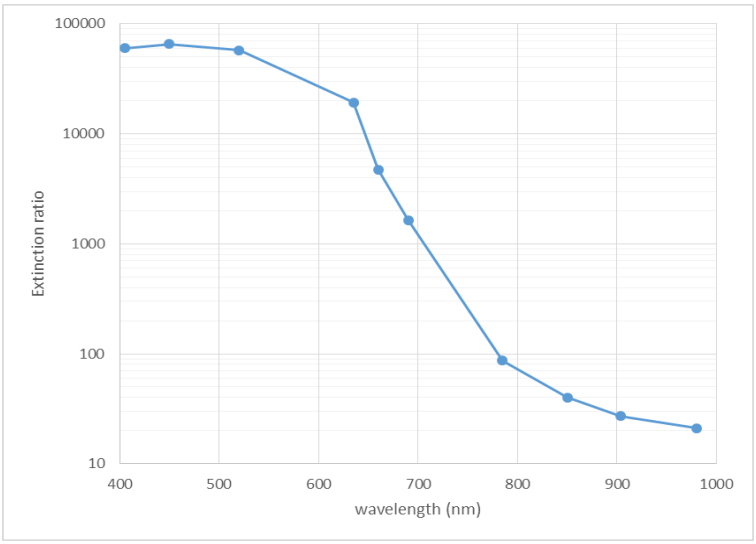

Figure 13 : OCAM2-S extinction ratio vs wavelength.

It would have been interesting to have measurements at ~600 nm but unfortunately there is no known laser diode available at this wavelength. The extinction ratio is in accordance with the theory for long wavelengths but higher than expected by one order of magnitude for shorter ones. This could be explained by a lower implant dose than expected and needs to be cross checked with E2V. But most likely the explanation would be a different working regime of the shutter system (different voltages) than the ones used for simulation and implant dose planning, resulting in better extinction ratios.

4. ON-SKY RESULTS WITH THE CANARY INSTRUMENT

4.1. The CANARY instrument

CANARY is the MOAO on-sky demonstrator installed at the William Herschel Telescope in the perspective of the future near-infrared multi-object integral field spectrograph instrument of the E-ELT [7]. It obtained the first demonstration of MOAO in open loop with three off-axis NGSs in 2010, using a 60cm sub-aperture sampling of the entrance pupil on the WFSs [8]. In the following phase, CANARY demonstrated the MOAO in open loop coupling both NGSs and LGSs [9]. The configuration was to add four Rayleigh off-axis LGSs to the three off-axis NGSs.

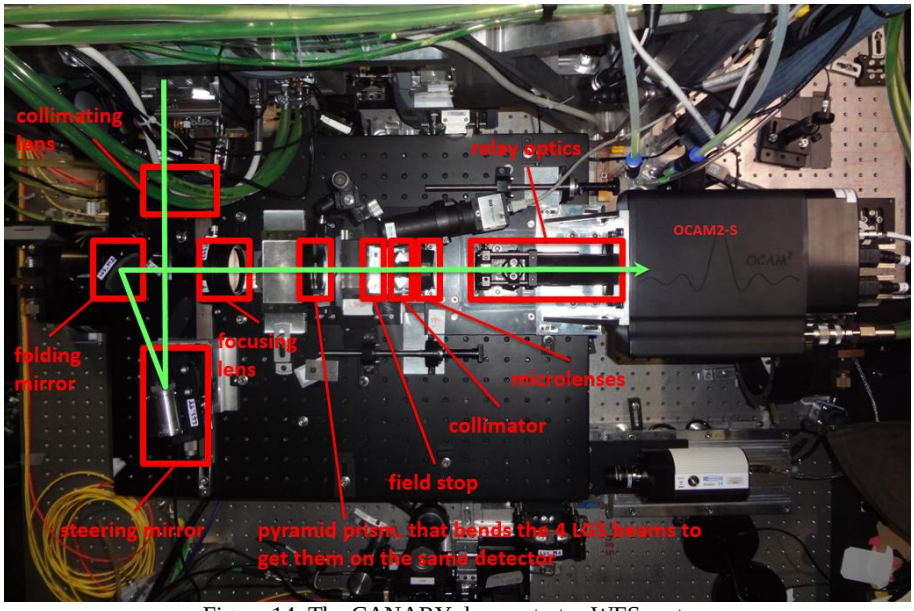

Figure 14: The CANARY demonstrator WFS system

4.2. On-Sky results

A major failure of the used gated CCD following this phase lead us to consider the implementation of the E2V CCD219 sensor with integral shutter capability. First tests were done in 2014 in LTAO mode having the deformable mirror in closed loop on all the L+NGS WFSs. We report here the late phase demonstration (in 2015) with the goal to mimic the two-stage AO correction configuration foreseen at the E-ELT, i.e. in CANARY having a first stage with a 8x8 actuator DM and a tip/tilt mirror in closed loop and a second stage in open loop simulating the MOAO channel to the spectrograph with a ALPAO 17x17 actuator deformable mirror. In CANARY, the four LGS Shack-Hartmann (SH) patterns are merged thanks to a pyramid on the unique CCD detector (OCAM2-S), see Figure 14 & 15.

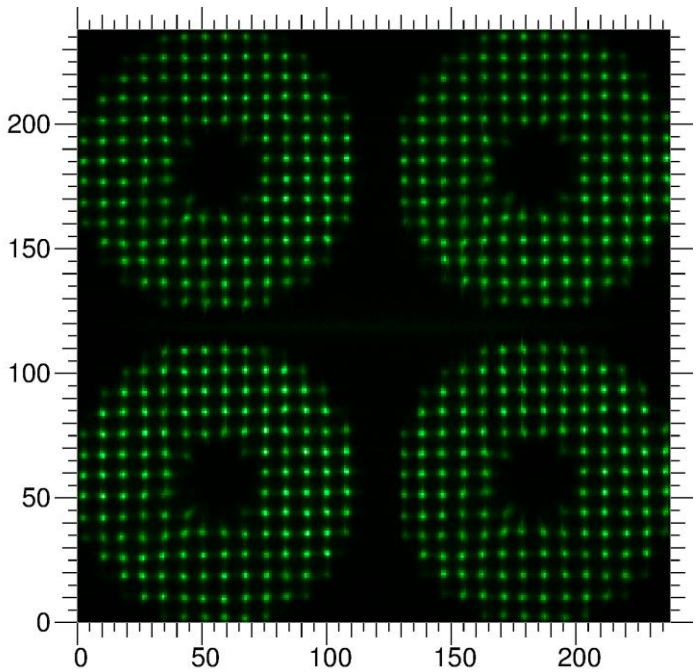

Figure 15: Shack-Hartmann patterns of the 4 Rayleigh LGS wavefront sensors imaged on the OCAM2-S camera using a temporal gate of 2 microseconds with a frame rate of 300Hz.

In this late phase, the pupil sampling was increased to a 14x14 SH for the LGSs to take advantage of the high order MOAO DM capability. The four Rayleigh LGS are formed at an altitude of 14km with a range gate of the 0.9 km and on a 23" radius asterism. The temporal gate on the detector is 6 microseconds with a laser pulse rate of 10kHz. The measured return flux from each range gated LGS is of the order of 162e-/subaperture/frame at 300 Hz frame rate for an output power to sky of approximately 4W per LGS.

During the two runs in 2015, in July and September, the OCAM2-S was perfectly operational allowing us to acquire a large sets of data, to test numerous AO configurations and to demonstrate the full tomography using a two stage correction mixing closed and open loop schemes and 4L + 3N off-axis GSs (see Gendron et al., 2015). We are currently reducing the data to analyse the performance achieved depending on the observing conditions.

5. CONCLUSION

With OCAM2-S we've successfully demonstrated the operation of a shuttered version of the OCAM2 camera. This gives a new outstanding tool in the adaptive optics scientists' toolbox. The performances are better than expected or simulated for both shutter response time and extinction ratio. As it is based on the well proven OCAM2 platform, the OCAM2-S camera is immediately available for on the sky production work. We have demonstrated its successful on-sky operation on the WHT telescope as an upgrade of the Rayleigh Laser Guide Star wavefront sensor of the CANARY instrument, which is a demonstrator for the E-ELT MOAO.

6. Acknowledgments

This work has been supported by EC FP7 OPTICON program, grants 211257 and 312430

REFERENCES

[1] P. Jerram, P. J. Pool, R. Bell, D. J. Burt, S. Bowring, S. Spencer, M. Hazelwood, I. Moody, N. Catlett, and P. S. Heyes, "The LLCCD: low-light imaging without the need for an intensifier", in Proc. SPIE, 4306, pp. 178-186, May 2001.

[2] P. Feautrier, J.L. Gach, P. Balard, C. Guillaume, M. Downing, N. Hubin, E. Stadler, Y. Magnard, M. Skegg, M. Robbins, S. Denney, W. Suske, P. Jorden, P. Wheeler, P. Pool, R. Bell, D. Burt, I. Davies, J. Reyes, M. Meyer, D. Baade, M. Kasper, R. Arsenault, T. Fusco, J. Javier Diaz-Garcia, "Characterization of OCam and CCD220: the fastest and most sensitive camera to date for AO wavefront sensing", in Proc. SPIE, 7736, June 2010.

[3] M. Downing, et. al., "A Dedicated L3Vision CCD for Adaptive Optics Applications", Scientific Detectors for Astronomy, 321-328 (2005).

[4] M. Downing, et. al., "Custom CCD for adaptive optics applications", Proc. SPIE 6276-19, Orlando (2006).

[5] J. Rose, S. Bradbury, I. Bond, P. Agden, A. Price, R. Oliver, Y. Khassen, "Driving LED in a nanosecond regime by a fast operational amplifier", arXiv:1011.1954 (2009)

[6] P. Feautrier, J.L.Gach "Visible and Infrared Wavefront Sensing detectors review in Europe - part I" In: Proceedings of the Third AO4ELT Conference. Firenze, Italy, 26-31 May 2013.

[7] Myers, R.M., et al., "CANARY: the on-sky NGS/LGS MOAO demonstrator for EAGLE" Proc. SPIE 7015, 70150E 1-9 (2008)

[8] Gendron, E., et al., "MOAO first on-sky demonstration with CANARY," A&A 529, L2 (2011)

[9] Morris, T., et al., "CANARY Phase B: On-sky open-loop tomographic LGS AO results" Proc. SPIE 9148, 91481I 1-12 (2014)

[10] Gendron, E., et al., "CANARY open loop demonstration: closed", in this AO4ELT conference (2015)